Au25: A Tip-enhanced, Spinning Top - Core-Shell? The Brightest Molecular Super Star Among the Nanoclusters, Au21-25(C1)

K. Vishwanathan (✉ vishwa_nathan_7@yahoo.com)

Saarland University

Au_{25}: A Tip-enhanced, Spinning Top - Core-Shell? The Brightest Molecular Super Star Among the Nanoclusters, $Au_{21-25}(C1)$

K. Vishwanathan[*]

Faculty of Natural Sciences and Technology, University of Saarland,
66123 Saarbrücken, Germany

Abstract

The geometries and vibrational frequency of the stable Au_N clusters with N = 21 to 25 are presented through the global structure re-optimization study. The finite-differentiation method has been implemented within the density-functional tight-binding (DFTB) approach. The effect of the range of interatomic forces was calculated and the desired set of system eigen-frequencies (3N-6) is obtained by diagonalization of the symmetric positive semidefinite Hessian matrix. We have observed the vibrational spectral ranges of between 2.88 and 328.25 cm^{-1} at $\Delta E = 0$, and even the minute details of the very lower frequencies were occupied in some clusters at the beginning of NVM itself which comes even below the scale of Far Infrared FIR, IR-C 200-10 cm^{-1}. Significantly, some of the clusters spectrums are with double state degeneracy and the rest of them are having single state degeneracy. Nevertheless, our investigation has revealed that the vibrational spectrum strongly depends upon the size, shape, and structure, as well as, stretching and bending vibrations of the atoms.

Keywords: Gold Atomic Clusters, Density-Functional Tight-Binding (DFTB) approach, Finite-Difference Method, Force Constants (FCs) and Vibrational Spectrum.

---

[*]Corresponding author. E-mail: vishwa_nathan_7@yahoo.com

1　Introduction

Noble metal nanoclusters are in the intermediate state between discrete atoms and plasmonic nanoparticles and are of significance due to their atomically accurate structures, intriguing properties, and great potential for applications in various fields. In addition, the size-dependent properties of nanoclusters construct a platform for thoroughly researching the structure (composition)-property correlations, which is favorable for obtaining novel nanomaterials with enhanced physicochemical properties. Thus far, more than 100 species of nanoclusters (mono-metallic Au or Ag nanoclusters, and bi-or tri-metallic alloy nanoclusters) with crystal structures have been reported. Among these nanoclusters, $Au_{25}(SR)_{18}$-the brightest molecular star in the nanocluster field is capable of revealing the past developments and prospecting the future of the nanoclusters. Since being successfully synthesized (in 1998, with a 20-year history) and structurally determined (in 2008, with a 10-year history), $Au_{25}(SR)_{18}$ has stimulated the interest of chemists as well as material scientists, due to the early discovery, easy preparation, high stability, and easy functionalization and application of this molecular star [1].

Remarkable recent advances on $Au_{25}(SR)_{18}$ nanoclusters have led to significant applications in catalysis, sensing, and magnetism. However, the existing synthetic routes are complicated, particularly for the water-soluble $Au_{25}(SG)_{18}$ nanoclusters. Sai Krishna Katla *etc.,* have reported a single-step concentration and temperature-controlled method for rapid synthesis of the $Au_{25}(SG)_{18}$ nanoclusters in as little as 2h without the need for low-temperature reaction or even stirring. A systematic time-based investigation was carried out to study the effects of volume, concentration, and temperature on the synthesis of these nanoclusters. Further, they have discovered for the first time that the $Au_{25}(SG)_{18}$ nanoclusters exhibit excellent photothermal activities in achieving 100 % cell death for MDA-MB-231 breast cancer cells at a power of 10 W/cm^2 using an 808 nm laser source, demonstrating applications toward photothermal therapy [2].

In general, nanoclusters are interesting because their physical, optical and electronic characteristics are strongly size dependent. Often changing the size by only one atom can significantly alter the physical chemical properties of the system [3], for that reasons, many new periodic tables can thus be envisioned classifying differently-sized clusters of the same material as new elements. Potential applications are enormous, ranging from devices in nano-electronics and nano-optics [4] to applications in medicine and materials. Gold colloids not only having some practical application recently, but also, have been used for centuries to stain glass which has been even used for the study of direct electrochemistry of proteins [5]. The main reasons are, gold is a soft metal and is usually alloyed to give it more strength. In addition to that gold is a good conductor of heat and electricity,

and is unaffected by air and most reagents. Noble-metal (Cu, Ag, and Au) clusters have attracted much attention in scientific and technological fields because of their thermodynamic, electronic, optical and catalytic properties in nano-materials [6, 7].

At peculiar stage, the vibrational properties play a major role in structural stability [8, 9, 10, 11, 12, 13, 14, 15]. The structural determination of metal nanoparticles of their vibrational (phonon) density of states have been calculated by Huziel E. Sauceda and Ignacio L. Garzón [14]. Specific heat capacity is an important thermodynamic property and is directly related to the structural stability, identification and energy of substances. Most recently, Huziel E. Sauceda and Ignacio L. Garzón [12] calculated vibrational properties and specific heat of core-shell Ag-Au icosahedral nanoparticles.

In this study, we focus on the vibrational properties of gold clusters with sizes Au_{21-25} atoms. Some general information about global minima gold structures which have been calculated by the work of Springborg and Dong [16, 17]. The structures were found through a so called *genetic algorithm* (GA) in combination with *Density Functional Tight-Binding* (DFTB) energy calculations and a *steepest descent* algorithm permitting a local total energy minimization. Nevertheless, in our case, we use our numerical finite-difference approach [18] along with density functional tight-binding (DFTB) method and extracted the vibrational spectrums. Overall, for a better understanding and to visualize, the detailed information is discussed in the results and discussion section.

The most important and deserving of attention; of consequence: these clusters are not crystallized, and our results are close to the 'Jellium' model.

2   Theoretical and Computational Procedure

At first, the DFTB [19, 20, 21] is based on the density functional theory of Hohenberg and Kohn in the formulation of Kohn and Sham. In addition, the Kohn-Sham orbitals $\psi_i(\mathbf{r})$ of the system of interest are expanded in terms of atom-centered basis functions $\{\phi_m(\mathbf{r})\}$,

$$\psi_i(\mathbf{r}) = \sum_m c_{im}\phi_m(\mathbf{r}), \quad m = j. \tag{1}$$

While so far the variational parameters have been the real-space grid representations of the pseudo wave functions, it will now be the set of coefficients c_{im}. Index m describes the atom, where ϕ_m is centered and it is angular as well as radially dependant. The ϕ_m is determined by self-consistent DFT calculations on isolated atoms using large Slater-type basis sets.

In calculating the orbital energies, we need the Hamilton matrix elements and the overlap matrix elements. The above formula gives the secular equations

$$\sum_m c_{im}(H_{mn} - \epsilon_i S_{mn}) = 0. \tag{2}$$

Here, c_{im}'s are expansion coefficients, ϵ_i is for the single-particle energies (or where ϵ_i are the Kohn-Sham eigenvalues of the neutral), and the matrix elements of Hamiltonian H_{mn} and the overlap matrix elements S_{mn} are defined as

$$H_{mn} = \langle \phi_m \mid \hat{H} \mid \phi_n \rangle, \quad S_{mn} = \langle \phi_m \mid \phi_n \rangle. \tag{3}$$

They depend on the atomic positions and on a well-guessed density $\rho(\mathbf{r})$. By solving the Kohn-Sham equations in an effective one particle potential, the Hamiltonian $\hat{H}$ is defined as

$$\hat{H}\psi_i(\mathbf{r}) = \epsilon_i \psi_i(\mathbf{r}), \quad \hat{H} = \hat{T} + V_{eff}(\mathbf{r}). \tag{4}$$

To calculate the Hamiltonian matrix, the effective potential V_{eff} has to be approximated. Here, $\hat{T}$ being the kinetic-energy operator $\sum(\hat{T} = -\frac{1}{2}\nabla^2)$ and $V_{eff}(\mathbf{r})$ being the effective Kohn-Sham potential, which is approximated as a simple superposition of the potentials of the neutral atoms,

$$V_{eff}(\mathbf{r}) = \sum_j V_j^0(\mid \mathbf{r} - \mathbf{R}_j \mid). \tag{5}$$

V_j^0 is the Kohn-Sham potential of a neutral atom, $\mathbf{r}_j = \mathbf{r} - \mathbf{R}_j$ is an atomic position, and $\mathbf{R}_j$ being the coordinates of the j-th atom.

Finally, the short-range interactions can be approximated by simple pair potentials, and the total energy of the compound of interest relative to that of the isolated atoms is then written as,

$$E_{tot} \simeq \sum_i \epsilon_i - \sum_j \sum_{m_j}^{occ} \epsilon_{jm_j} + \frac{1}{2}\sum_{j \neq j'} U_{jj'}(\mid \mathbf{R}_j - \mathbf{R}_{j'} \mid),$$
$$\epsilon_B \equiv \sum_i \epsilon_i - \sum_j \sum_{m_j}^{occ} \epsilon_{jm_j} \tag{6}$$

Here, the majority of the binding energy (ϵ_B) is contained in the difference between the single-particle energies ϵ_i of the system of interest and the single-particle energies ϵ_{jm_j} of the isolated atoms (atom index j, orbital index m_j), $U_{jj'}(\mid \mathbf{R}_j - \mathbf{R}_{j'} \mid)$ is determined as the difference between ϵ_B and ϵ_B^{SCF} for diatomic molecules (with E_B^{SCF} being the total energy from parameter-free density-functional calculations). In the present study, only the $5d$ and $6s$ electrons of the

4

gold atoms are explicitly included, whereas the rest are treated within a frozen-core approximation [19, 21, 22].

2.1 Structural re-optimization process

In our case, we have calculated the numerical first-order derivatives of the forces $(\mathbf{F}_{i\alpha}, \mathbf{F}_{j\beta})$ instead of the numerical-second-order derivatives of the total energy (E_{tot}). In principle, there is no difference, but numerically the approach of using the forces is more accurate [18],

$$\frac{1}{M}\frac{\partial^2 E_{tot}}{\partial \mathbf{R}_{i\alpha}\partial \mathbf{R}_{j\beta}} = \frac{1}{M}\frac{1}{2ds}\left[\frac{\partial}{\partial \mathbf{R}_{i\alpha}}(\text{-}\mathbf{F}_{j\beta}) + \frac{\partial}{\partial \mathbf{R}_{j\beta}}(\text{-}\mathbf{F}_{i\alpha})\right] \tag{7}$$

Here, F is a restoring forces which is acting upon the atoms, ds is a differentiation step-size and M represents the atomic mass, for homonuclear case. The complete list of these force constants (FCs) is called the Hessian H, which is a $(3N \times 3N)$ matrix. Here, i is the component of (x, y or z) of the force on the j'th atom, so we get $3N$.

2.1.1 The Hessian Matrix

The Hessian matrix is the matrix of second derivatives of the energy with respect to geometry which is quite sensitive to its geometry. Energy second derivatives are evaluated numerically. The mass-weighted Hessian matrix is obtained by numerical differentiation of the analytical first derivatives, calculated at geometries obtained by incrementing in turn each of the $3N$ nuclear coordinates by a small amount ds with respect to the equilibrium geometry. The introduction of the Hessian matrix and its diagonalization ultimately leads to the eigen-frequencies of the system and its eigenvectors, describing the harmonic motion of the clusters atoms. In order to obtain the matrix elements H_{ij} of the Hessian matrix which are needed if one wishes to investigate the clusters thermodynamic properties and one should obtain the derivatives of potential energy surface (**PES**) [17, 23].

3 Results and Discussion

3.1 The optimized structure of the cluster Au_{21-25}

We present a vibrational spectrum analysis of re-optimized Au_{21-25} cluster, very interestingly, almost all of them are having with a group symmetry C_1 at $\Delta E = 0$. Initially, the structures were found through a so called *genetic algorithm* (GA) in combination with *Density Functional Tight-Binding* (DFTB) energy calculations and a *steepest descent* algorithm permitting a local total energy minimization [16].

To sum up, we have accurately predicted the vibrational frequencies of the clusters, and they are very strongly depend on the size, structure and shape of the clusters, as well as, mainly influenced by the stretching and the bending mode vibrations of the atoms that is due to a changes on the bond length fluctuations for a small step-size $ds = \pm 0.01$ a.u. on the equilibrium coordinates. For the perspective view, we have plotted with two different style (Space-filling, Polyhedral). Figs 1-5. clearly shows the standard orientation of crystal shape of the clusters $Au_{21-25}(C_1)$ at $\Delta E = 0$ (the lowest energy geometrical structure). In addition to that these clusters are not crystallized, and our results are closely related to the 'Jellium' model [24].

3.1.1 The vibrational frequency (ω_i) range of the cluster Au_{21} at $\Delta E = 0$

Table 1 shows that the low (at the least) and the high (at the most) frequency range of cluster Au_{21}. The lowest and the highest frequency range in between 4.58 cm^{-1} to 284.41 cm^{-1}.

Firstly, the cluster has some low frequencies (ω_{min}) in between 4.58-9.90 cm^{-1}, that is only for the very first 4 NVM, which comes even below the scale of Far Infrared FIR, IR-C 200-10 cm^{-1}.

Secondly, for the 5-48 NVM, the frequency ranges are occurred in between 14.34-193.50 cm^{-1}, which comes within the range of Far Infrared FIR, IR-C 200-10 cm^{-1}.

Thirdly, for the rest of the 49-57 NVM, are having the maximum high frequencies, which are ((ω_i) - 200.03-284.41 cm^{-1}) falling within the range of Mid Infrared MIR, IR-C 3330-200 cm^{-1}.

The double and the single state degeneracy: At NVM 36, 37 that gives only one pair of degeneracy (120.82, 120.91 cm^{-1}) that has occurred within the range of Far Infrared FIR, IR-C 200-10 cm^{-1}. Surely, such kind of spectrum could be highly possible to observe in the experimental calculations.
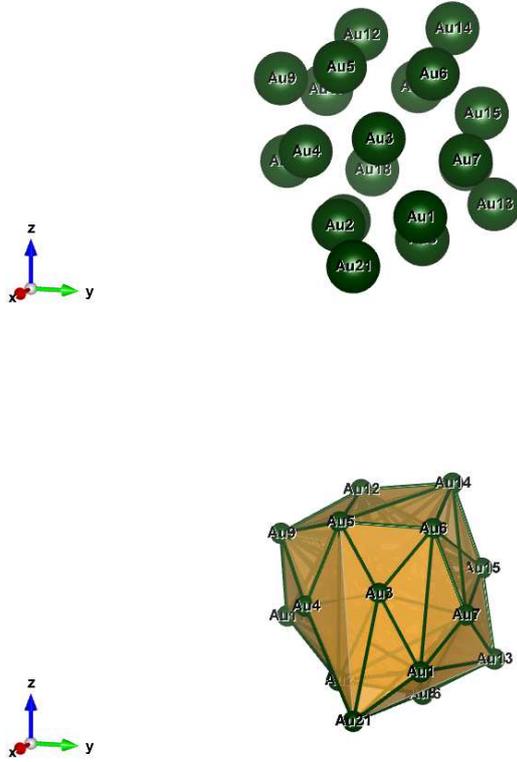
Figure 1: Au_{21} (C_1); Style (Space-filling [above], Polyhedral [below]): The lowest energy geometrical structures of the Au_{21} cluster. Standard orientation of crystal shape at $\Delta E = 0$.

3.1.2 The vibrational frequency (ω_i) range of the cluster Au_{22} at $\Delta E = 0$

Table 2 shows that the low (at the least) and the high (at the most) frequency range of cluster Au_{22}. The lowest and the highest frequency range in between 6.09 cm^{-1} to 308.42 cm^{-1}.

Firstly, the cluster has some low frequencies (ω_{min}) in between 6.09-9.25 cm^{-1}, that is only for the very first 4 NVM, which comes even below the scale of Far Infrared FIR, IR-C 200-10 cm^{-1}.

Secondly, for the 5-48 NVM, the frequency ranges are occurred in between 12.93-196.20 cm^{-1}, which comes within the range of Far Infrared FIR, IR-C 200-10 cm^{-1}.

Thirdly, for the rest of the 49-60 NVM, are having the maximum high frequen-

7

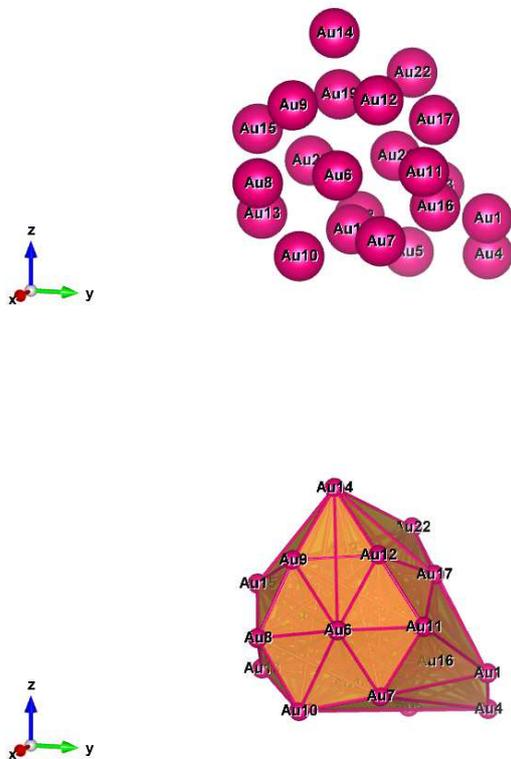Figure 2: Au$_{22}$ (C_1); Style (Space-filling [above], Polyhedral [below]): The lowest energy geometrical structures of the Au$_{22}$ cluster. Standard orientation of crystal shape at $\Delta E = 0$.

cies, which are ((ω_i) - 202.22-308.42 cm^{-1}) falling within the range of Mid Infrared MIR, IR-C 3330-200 cm^{-1}.

The double and the single state degeneracy: At NVM 2, 3 that gives only one pair of degeneracy (7.06, 7.35 cm^{-1}) that has occurred below the scale of Far Infrared FIR, IR-C 200-10 cm^{-1}. Probably, such kind of spectrum may be possible, if not, it will be silent to observe in the experimental calculations.

3.1.3 The vibrational frequency (ω_i) range of the cluster Au_{23} at $\Delta E = 0$

Table 3 shows that the low (at the least) and the high (at the most) frequency range of cluster Au_{23}. The lowest and the highest frequency range in between 2.88 cm^{-1} to 295.85 cm^{-1}.
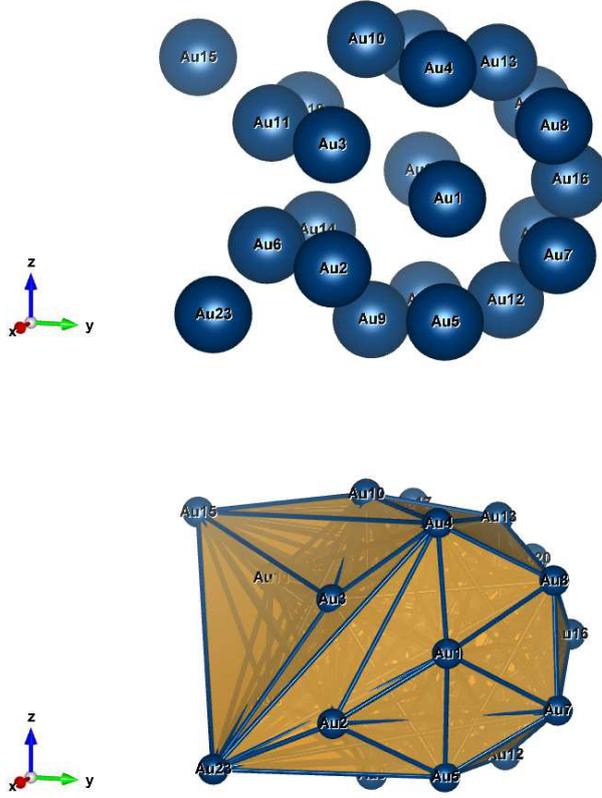
8

Figure 3: Au$_{23}$ (C_1); Style (Space-filling [above], Polyhedral [below]): The lowest energy geometrical structures of the Au$_{23}$ cluster. Standard orientation of crystal shape at $\Delta E = 0$.

Firstly, the cluster has some low frequencies (ω_{min}) in between 2.88-8.11 cm^{-1}, that is only for the very first 3 NVM, which comes even below the scale of Far Infrared FIR, IR-C 200-10 cm^{-1}.

Secondly, for the 4-51 NVM, the frequency ranges are occurred in between 10.78-194.04 cm^{-1}, which comes within the range of Far Infrared FIR, IR-C 200-10 cm^{-1}.

Thirdly, for the rest of the 52-63 NVM, are having the maximum high frequencies, which are ((ω_i) - 203.12-295.85 cm^{-1}) falling within the range of Mid Infrared MIR, IR-C 3330-200 cm^{-1}.

The double and the single state degeneracy: At NVM 6, 7 and 11, 12 that gives two pairs of degeneracy ({16.06, 16.99; 23.42, 23.67} cm^{-1}) that has occurred within the range of Far Infrared FIR, IR-C 200-10 cm^{-1}. Surely, such kind

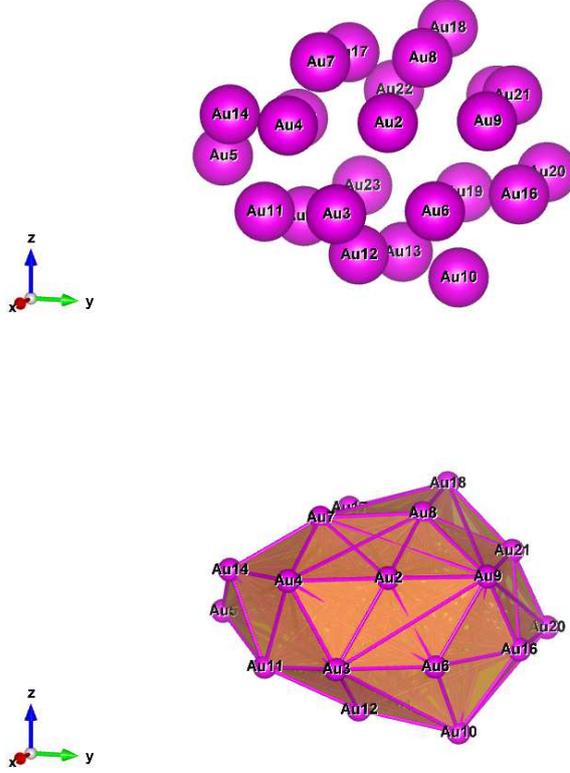of spectrum could be highly possible to observe in the experimental calculations.

Figure 4: Au$_{24}$ (C_1); Style (Space-filling [above], Polyhedral [below]): The lowest energy geometrical structures of the Au$_{24}$ cluster. Standard orientation of crystal shape at $\Delta E = 0$.

3.1.4   The vibrational frequency (ω_i) range of the cluster Au_{24} at $\Delta E = 0$

Table 4 shows that the low (at the least) and the high (at the most) frequency range of cluster Au_{24}. The lowest and the highest frequency range in between 6.98 cm^{-1} to 295.86 cm^{-1}.

Firstly, the cluster has some low frequencies (ω_{min}) in between 6.98-8.52 cm^{-1}, that is only for the very first 2 NVM, which comes even below the scale of Far Infrared FIR, IR-C 200-10 cm^{-1}.

Secondly, for the 3-52 NVM, the frequency ranges are occurred in between

10.36-194.03 cm^{-1}, which comes within the range of Far Infrared FIR, IR-C 200-10 cm^{-1}.

Thirdly, for the rest of the 53-66 NVM, are having the maximum high frequencies, which are ((ω_i) - 201.84-295.86 cm^{-1}) falling within the range of Mid Infrared MIR, IR-C 3330-200 cm^{-1}.

The double and the single state degeneracy: At NVM 7, 8 that gives only one pair of degeneracy (17.15, 17.50 cm^{-1}) that has occurred within the range of Far Infrared FIR, IR-C 200-10 cm^{-1}. Surely, such kind of spectrum could be highly possible to observe in the experimental calculations.
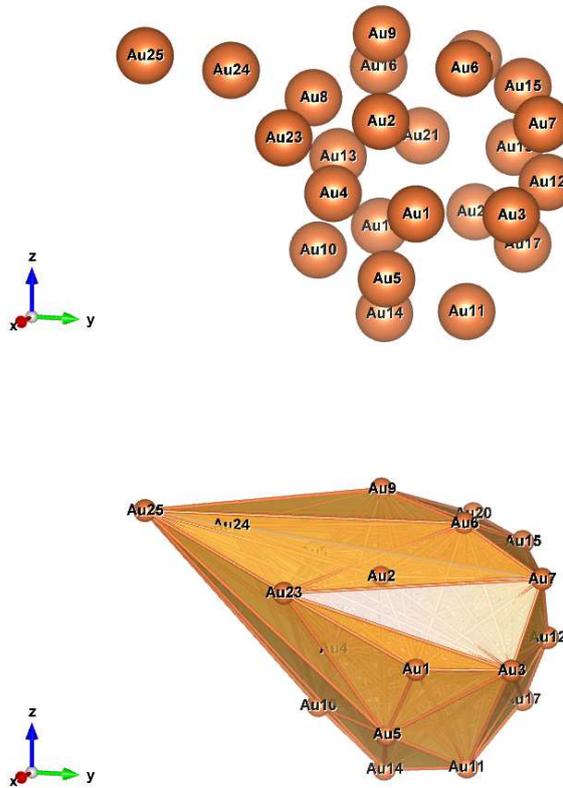

Figure 5: Au_{25} (C_1); Style (Space-filling [above], Polyhedral [below]): The lowest energy geometrical structures of the Au_{25} cluster. Standard orientation of crystal shape at $\Delta E = 0$.

3.1.5 The vibrational frequency (ω_i) range of the cluster Au_{25} at $\Delta E = 0$

Table 5 shows that the low (at the least) and the high (at the most) frequency range of cluster Au_{25}. The lowest and the highest frequency range in between 3.89 cm^{-1} to 328.25 cm^{-1}.

Firstly, the cluster has some low frequencies (ω_{min}) in between 3.89-7.25 cm^{-1}, that is only for the very first 4 NVM, which comes even below the scale of Far Infrared FIR, IR-C 200-10 cm^{-1}.

Secondly, for the 5-53 NVM, the frequency ranges are occurred in between 10.06-196.60 cm^{-1}, which comes within the range of Far Infrared FIR, IR-C 200-10 cm^{-1}.

Thirdly, for the rest of the 54-69 NVM, are having the maximum high frequencies, which are ((ω_i) - 204.88-328.25 cm^{-1}) falling within the range of Mid Infrared MIR, IR-C 3330-200 cm^{-1}.

The double and the single state degeneracy: There are no double state degeneracy but all of the spectra are having only a single state degeneracy, as a result, that gives an excellent structural view, the details are in the below descriptions.

A Spinning Top and the Core-Shell of Au_{25}: In general, a spinning top, or simply a top, is a toy with a squat body and a sharp point at the bottom, designed to be spun on its vertical axis, balancing on the tip due to the gyroscopic effect [25]. Surprisingly, our sky-line (outline) shape of the cluster resembles the very same as spinning-top (see Fig. 5), as well as having the core-shell at the centered, and it is being visible through the perspective structural view.

Recently, in the review and the research work of Xi Kang and Sai Krishna Katla *etc.,*, have dealt a detailed information about the hybridization for the cluster Au_{25} in the nanocluster field and is capable of revealing the past developments and prospecting the future of the nanoclusters [1, 2]. Additionally, in the review of Xi Kang *etc.,*, the preparation methods, crystal structures, physicochemical properties, and practical applications of $Au_{25}(SR)_{18}$ are summarized. The properties of $Au_{25}(SR)_{18}$ range from optics and chirality to magnetism and electrochemistry, and the property-oriented applications include catalysis, chemical imaging, sensing, biological labeling, biomedicine and beyond. Furthermore, the research progress on the Ag-based $M_{25}(SR)_{18}$ counterpart (*i.e.,* $Au_{25}(SR)_{18}$) is included in their review due to its homologous composition, construction and optical absorption to its gold-counterpart $Au_{25}(SR)_{18}$. Moreover, the alloying methods, metal-exchange sites and property alternations based on the templated $Au_{25}(SR)_{18}$ are highlighted. Finally, some perspectives and challenges for the future research of the $Au_{25}(SR)_{18}$ nanocluster are proposed (also holding true for all members in the nanocluster field) [1].

Advantage and the future usages: Due to the excellence nature of the physical

structure, very significantly, one of the atom Au_{25} is located at the corner or spin top, as a tip of the whole core-shell-structure that can easily helps to connect with any other possible molecules with ligand or catalyst, as a result, that will lead to produce a new bioelectronics, nano electric devices *etc.,*. It is not being found at any other clusters, so far !.

In our case, mainly, on the clusters, the degree of degeneracy is being released due to the bond length fluctuation of the symmetric as well as anti-symmetric move of the atoms. Additionally, for understanding and describing the atomic interactions in the cluster [26, 27, 28, 29, 30, 31], one must have the basic knowledge of, if the energy absorbed when bond breaks, at the same time, the energy released when bond forms. When increase the bond length then bond strength will become weaker but if we bring closer the bond length to each other, as a result, the bond strength will become stronger. We can observe attraction with a shared electrons as well as repulsion due to nuclei and electron shell.

Surely, the ab initio calculations performed within this study confirm the theoretical and the experimental results: The most stable configuration of the cluster is not crystalline but with a high probability this cluster is a shapeless. This cluster was composed of two shells surrounding a central atom. Furthermore, a shell structure should not be considered as a kind of ordering in the context of small nanoparticles. Even the random arrangement of gold atoms, used as starting condition for some of the calculations, shows such a shell structure. We conclude that, the highest probability of the lowest energy structure for can be amorphous (as non-crystalline), which is an excellent agreement with the conclusion of the known results [32, 33, 34, 35].

3.1.6   Jellium model comparison with our results:

The jellium model of simple metal clusters has enjoyed remarkable empirical success, leading to many theoretical questions. In Matthias Brack review [24], they first survey the hierarchy of theoretical approximations leading to the model. They then described the jellium model in detail, including various extensions. One important and useful approximation is the local-density approximation to exchange and correlation effects, which greatly simplifies self-consistent calculations of the electronic structure. Another valuable tool is the semiclassical approximation to the single-particle density matrix, which gives a theoretical framework to connect the properties of large clusters with the bulk and macroscopic surface properties. The physical properties discussed in that review are the ground-state binding energies, the ionization potentials, and the dipole polarizabilities. They also treated the collective electronic excitations from the point of view of the cluster response, including some useful sum rules [24, 36]. In this connection, they have found that the jellium model is a useful mediator between the microcosm and the macrocosm.

13

Nevertheless, only the temperature of the electrons can be treated rigorously in the jellium model; the ions are not accessible microscopically. This is a serious restriction, since a dominant fraction of the thermal energy in cluster beams is carried by the ions. However, the ionic part of the thermal energy can be assumed to be a smooth function of the particle number. Therefore the shell-structure oscillations coming from the valence electrons and their temperature dependence can also be studied in the jellium model [24].

In many experiments, clusters are produced at finite temperatures of up to several hundred Kelvin or even more [24, 36]. The manifestation of shell structure in the abundance spectra of cluster-beam experiments is thought to be a result of evaporation of neutral atoms by the hot clusters: the closer the number of valence electrons gets to a number corresponding to a filled major shell, the more stable the cluster will be and the smaller the probability for evaporation of a further atom, so that finally at the time of detection-when the beam has cooled off-the closed-shell species are the most abundant [24, 37].

The question therefore arises to what extent a finite temperature affects the magnitude of the electronic shell effects themselves. Shell effects are weakened at finite temperature for two reasons. Most of the excitation energy will be in the structural degrees of freedom, namely , in the vibrations, distortions, and lique-faction of the cluster. The amount of phase space associated with high symmetry shapes that produce electronic shell closures will then be reduced. Independent of this, the occupation of the electronic orbitals will be smeared out as in the Fermi-Dirac distribution. This will also smooth out shell effects, as is well known from nuclear physics [24, 38, 39].

At first sight, one might think that even several hundred degrees are small on the scale of the electronic single-particle energies, so that this second effect should be negligible. This is certainly true for clusters with fewer than a hundred atoms in which the main spacing between electronic levels corresponds to several thousand degrees. However, in very large clusters in the mass region $N \simeq 1000$-3000, which now have become available in expansion sources, the spectra are much more compressed and the temperatures in question do have a noticeable effect. Furthermore, the detailed shape of the abundance spectra depends in a rather subtle way on first and second differences of the total free energies with respect to the atomic number, so that the temperature smearing effects can, indeed, become visible [24, 40, 41]. Our model and its details have been described in section 2.

4   Conclusion

We have extracted the vibrational frequency of medium-sized clusters (Au_{21-25}) the shell-like structure (of course, they are part of the family of so-called full-

shell clusters) at $\Delta E = 0$ by using the numerical finite-differentiation with DFTB method. The present calculations of the frequency spectrum are predictions to be confirmed when the experimental data become available. The Hessian matrix, calculated to obtain the normal modes of vibration in this work, can be much useful in MD simulations which can find a dependency of the gold atomic cluster assisted catalytic process on temperature. We have observed the vibrational properties of the clusters in order to explore the interaction between stability and the structure of clusters. Our new approach is worthy of further investigation and would pave a way in realizing numerical values which would allow for an experimental vibrational spectrum, which would prove crucial in the development of nanoelectronic devices. Nevertheless, our work gives a possible cause for the size and structure effect of Au atomic clusters.

Last but not least, our present study gives additional support to the prediction of the existence of shapeless stable structures in metal clusters. The appearance of such structures will always depend on the range of the n-body interaction responsible for the metallic cohesion in these systems. As a consequence, the existence of amorphous clusters does not depend on the use of any specific model potential but on the range and screening of the collective interaction between nuclei and electrons. Above all, these clusters are not crystallized, and our results are close to the 'Jellium' model.

5 Corresponding authors

Correspondence to K. Vishwanathan, E-mail: vishwa_nathan_7@yahoo.com; Ph. No. + 49-0151-63119680.

6 Data Availability

Source data for Table 1-5 is provided with the paper.

7 Acknowledgements

References

[1] $Au_{25}(SR)_{18}$: the captain of the great nanocluster ship, Xi Kang, Hanbao Chonga and Manzhou Zhu, Nanoscale, 10, 10758-10834, 2018. https://doi.org/10.1039/C8NR02973C

[2] Atomically Precise $Au_{25}(SG)_{18}$ Nanoclusters: Rapid Single-Step Synthesis and Application in Photothermal Therapy, Sai Krishna Katla, Jie Zhang, Edison Castro, Ricardo A. Bernal, and XiuJun Li, ACS Appl. Mater. Interfaces, 10, 1, 2018.

[3] Liangliang Wu, Weihai Fang & Xuebo Chen, The photoluminescence mechanism of ultra-small gold clusters. *Phys. Chem. Chem. Phys.* **18**, 17320-17325 (2016) DOI: 10.1039/C6CP02770A.

[4] Andres, R. P., Bein, T., Dorogi, M., Feng, S., Henderson, J. I., Kubiak, C. P., Mahoney, W., Osifchin, R. G. & Reifenberger, R., Coulomb Staircase at Room Temperature in a Self-Assembled Molecular Nanostructure. *Science* **272**, 1323-1325, (1996).

[5] Kamat P.V. Photophysical, Photochemical and Photocatalytic Aspects of Metal Nanoparticles. J. Phys. Chem. B. 106:7729-7744, (2002). doi: 10.1021/jp0209289.

[6] Li, J., Liu, Y., Zhang, J., Liang, X. and Duan, H. Density functional theory study of the adsorption of hydrogen atoms on Cu_2X (X = 3d) clusters. Chem. Phys. Lett. 651, 137-143, https://doi.org/10.1016/j.cplett.2016.03.035 (2016).

[7] Static and dynamical isomerization of Cu_{38} cluster Chuanchuan Zhang, Haiming Duan, Xin Lv, Biaobing Cao, Ablat Abliz, Zhaofeng Wu & Mengqiu Long, Scientific Reports, 9:7564, (2019) https://doi.org/10.1038/s41598-019-44055-z.

[8] Ignacio L. Garzón and Alvaro Posada-Amarillas, Structural and vibrational analysis of amorphous Au$_{55}$ clusters, *Phys. Rev. B.,* **54**, 11796, (1996).

[9] G. Bravo-Perez, I. L. Garzón and O. Novaro, An initio study of small gold clusters, *THEOCHEM.,* **493,** 225-231, (1999).

[10] G. Bravo-Perez, I. L. Garzón and O. Novaro, Non-additive effects in small gold clusters, *Chem. Phys. Lett.,* **313,** 655-664, (1999).

[11] H. E. Sauceda, D. Mongin, P. Maioli, A. Crut, M. Pellarin, N. del Fatti, F. Vallée, I. L. Garzón, Vibrational properties of metal nanoparticles: atomistic simulation and comparison with time-resolved investigation, *J. Phys. Chem. C.,* **116,** 25147, (2012).

[12] H. E. Sauceda, J. J. Pelayo, F. Salazar, L. A. Pérez, I. L. Garzón, Vibrational spectrum, caloric curve, low-temperature heat capacity, and Debye temperature of sodium clusters: The Na139+ case, *J. Phys. Chem. C.,* **117,** 11393, (2013).

[13] H. E. Sauceda, F. Salazar, L. A. Pérez, I. L. Garzón, Size and shape dependence of the vibrational spectrum and low-temperature specific heat of Au nanoparticles, *J. Phys. Chem. C.,* **117,** 25160, (2013).

[14] H. E. Sauceda and I. L. Garzón, Structural determination of metal nanoparticles from their vibrational (phonon) density of states, *J. Phys. Chem. C.,* **119,** 10876, (2015).

[15] N. Dugan, S. Erkoc, *Phys. Stat. Sol. B.,* **245**, 695, (2008).

[16] Y. Dong & M. Springborg, Global structure optimization study on Au_{2-20}, *Eur. Phys. J. D.* **43**, 15-18 (2007).

[17] Heat Capacities of Metal Clusters, Diploma Thesis (Research Assistant and Diploma Research), Saarland University, 2007.

[18] M. Dvornikov. Formulae of numerical differentiation. Preprint, arXiv:math.NA/0306092v3, (2004).

[19] D. Porezag, Th. Frauenheim, Th. Köhler, G. Seifert & R. Kaschner, Construction of tight-binding-like potentials on the basis of density-functional theory: Application to carbon. *Phys. Rev. B.* **51**, 12947 (1995).

[20] G. Seifert & R. Schmidt, Molecular dynamics and trajectory calculations: the application of an LCAO-LDA scheme for simulatins of cluster-cluster collisions. *New J. Chem.* **16**, 1145 (1992).

[21] G. Seifert, D. Porezag & Th. Frauenheim, Calculations of molecules, clusters, and solids with a simplified LCAO-DFT-LDA scheme. *Int. J. Quantum Chem.* **58**, 185-192 (1996)

[22] G. Seifert, Tight-Binding Density Functional Theory: An Approximate Kohn-Sham DFT Scheme. *J. Phys. Chem. A.* **111**, 5609-5613 (2007).

[23] W. H. Press, S. A. Teukolsky, W. T. Vetterling, and B. P Flannery. Numerical Recipes in Fortran. Cambridge University Press (2007).

[24] The physics of simple metal clusters: self-consistent jellium model and semi-classical approaches, Matthias Brack, Rev. Mod. Phys. , Vol. 65, No. 3, (1993).

[25] H. Crabtree (1909). An Elementary Treatment of the Theory of Spinning Tops and Gyroscopic Motion. London: Longman, Green and C.

[26] D. J. Wales, Frontiers Article: Surveying a Complex Potential Energy Landscape: Overcoming Broken Ergodicity Using Basin-Sampling, *Chem. Phys. Lett.,* **584,** 1-9, (2013).

[27] A. J. Ballard, S. Martiniani, J. D. Stevenson, S. Somani and D. J. Wales, Wiley Interdisciplinary Reviews: *Computational Molecular Science.,* **5**, 273-289, (2015).

[28] Stefano Martiniani, Jacob D. Stevenson, David J. Wales, and Daan Frenkel, Superposition Enhanced Nested Sampling, *Phys. Rev. X.,* **4,** 031034, (2014).

[29] Mandelshtam, V. A. and Frantsuzov, P. A. and Calvo, F, Structural Transitions and Melting in LJ 7 4 - 7 8 Lennard-Jones Clusters from Adaptive Exchange Monte Carlo Simulations, *J. Phys. Chem. A.,* **110,**, 5326-5332, (2006).

[30] Sharapov, V. A. and Mandelshtam, V. A., Solid-Solid Structural Transformations in Lennard-Jones Clusters: Accurate Simulations versus the Harmonic Superposition Approximation., *J. Phys. Chem. A.,* **111,** 10284-10291, (2007).

[31] Sharapov, V. A. and Meluzzi, D. and Mandelshtam, V. A., Low-temperature structural transitions: Circumventing the broken-ergodicity problem, *Phys. Rev. Lett.,* **98,** 105701, (2007).

[32] Structural Evolution of Medium-Sized Gold Clusters Au_n (n=36, 37, 38): Appearance of Bulk-Like Face Centered Cubic Fragment, Nan Shao, Wei Huang, Wai-Ning Mei, Lai Sheng Wang, Qin Wu,and Xiao Cheng Zeng, J. Phys. Chem. C, 118, 6887-6892, (2014).

[33] Doye, J. P. & Wales, D. J. Global minima for transition metal clusters described by Sutton–Chen potentials. New Journal of Chemistry, 22(7), 733-744, (1998).

[34] Huang, W., Ji, M., Dong, C. D., Gu, X., Wang, L.M., Gong, X.G. & Wang, L.S. Relativistic effects and the unique low-symmetry structures of gold nanoclusters. ACS Nano, 2(5), 897-904, (2008).

[35] Wang, L. M. & Wang, L. S. Probing the electronic properties and structural evolution of anionic gold clusters in the gas phase. Nanoscale, 4(14), 4038-4053, (2012).

[36] de Heer, W. A., Rev. Mod. Phys. 65, 611, (1993).

[37] Bjørnholm, S., T. Døssing, K. Hansen, and H. Nishioka, 1993, Phys. Rep. (in press).

[38] Bohr, A., and B. Mottelson, (1975) Nuclear Structure 2 (Benjamin, New York).

[39] Brack, M., and P. Quentin, Nucl. Phys. A 361, 35 (1981).

[40] Bjørnholm, S., J. Borggreen, O. Echt, K. Hansen, J. Pedersen, and H. D. Rasmussen, Z. Phys. D 19, 47 (1991).

[41] Pedersen, 3., S. Bjørnholm, J. Borggreen, K. Hansen, T. P. Martin, and H. D. Rasmussen, Nature 353, 733 (1991).

Figures
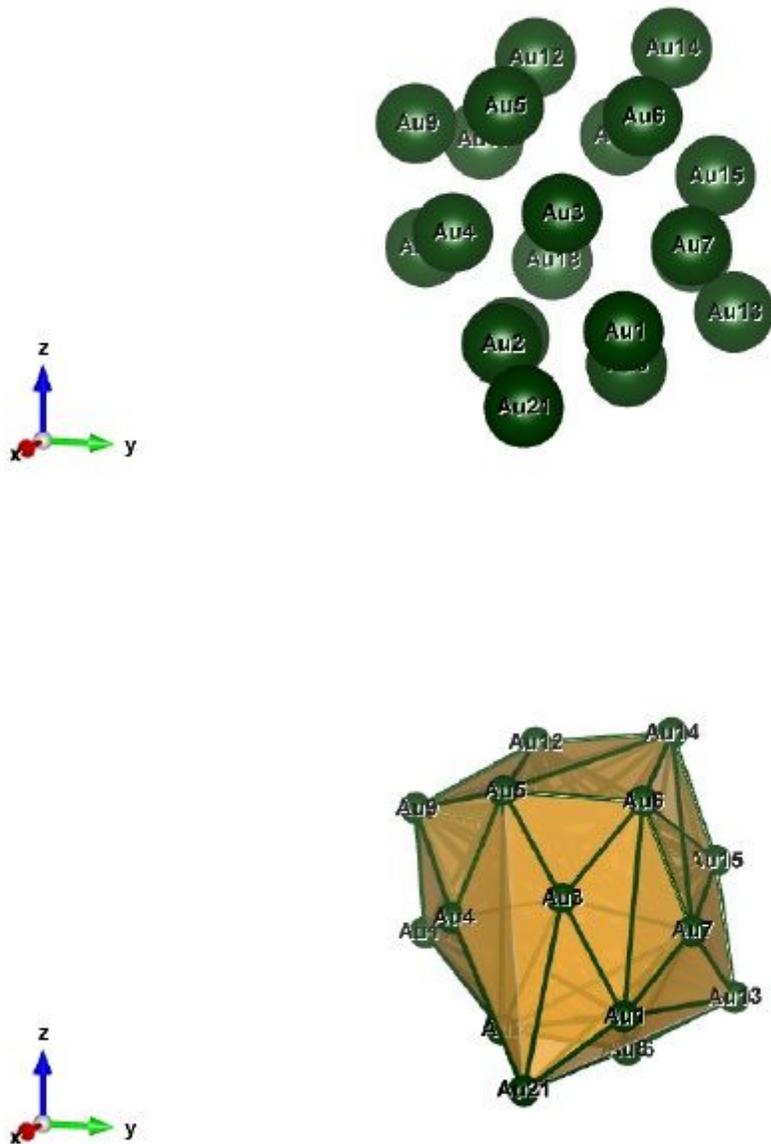
Figure 1

Au21 (C1); Style (Space-lling [above], Polyhedral [below]): The lowest energy geometrical structures of the Au21 cluster. Standard orientation of crystal shape at ΔE = 0.
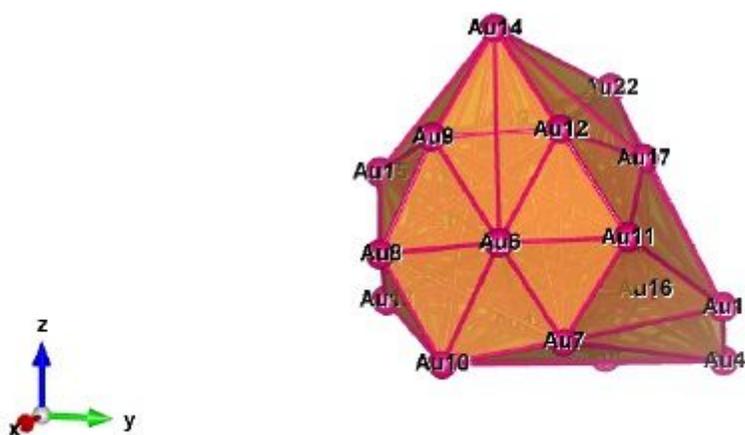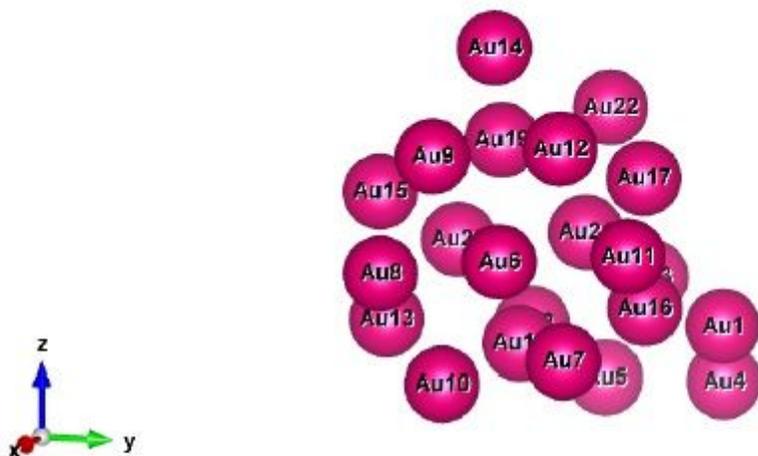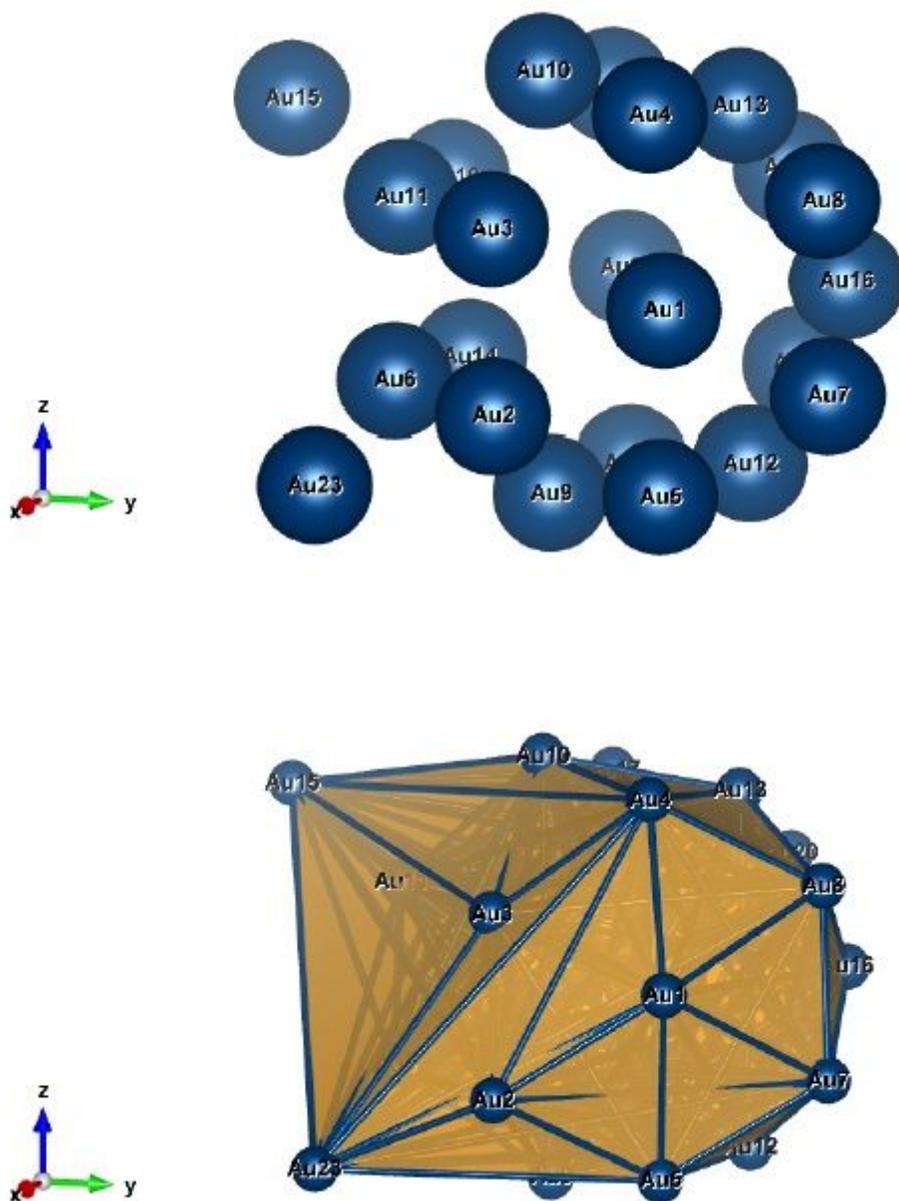
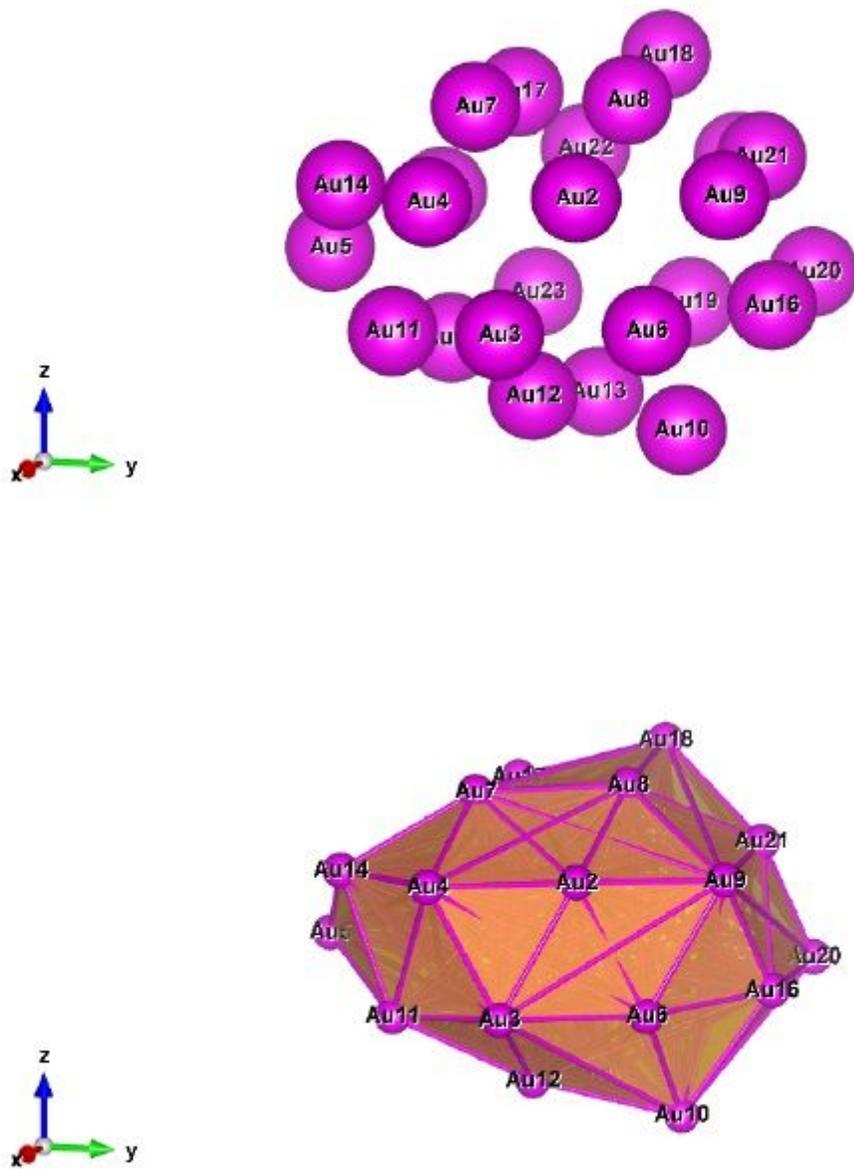**Figure 2**

Au22 (C1); Style (Space-lling [above], Polyhedral [below]): The lowest energy geometrical structures of the Au22 cluster. Standard orientation of crystal shape at ⊿E = 0.
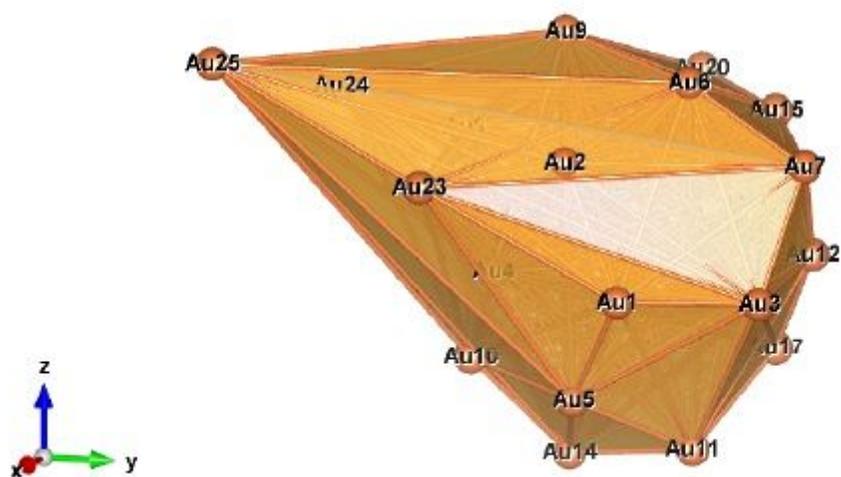
Figure 3

Au23 (C1); Style (Space-lling [above], Polyhedral [below]): The lowest energy geometrical structures of the Au23 cluster. Standard orientation of crystal shape at $\Delta E = 0$.

Figure 4

Au24 (C1); Style (Space-lling [above], Polyhedral [below]): The lowest energy geometrical structures of the Au24 cluster. Standard orientation of crystal shape at $\Delta E = 0$.
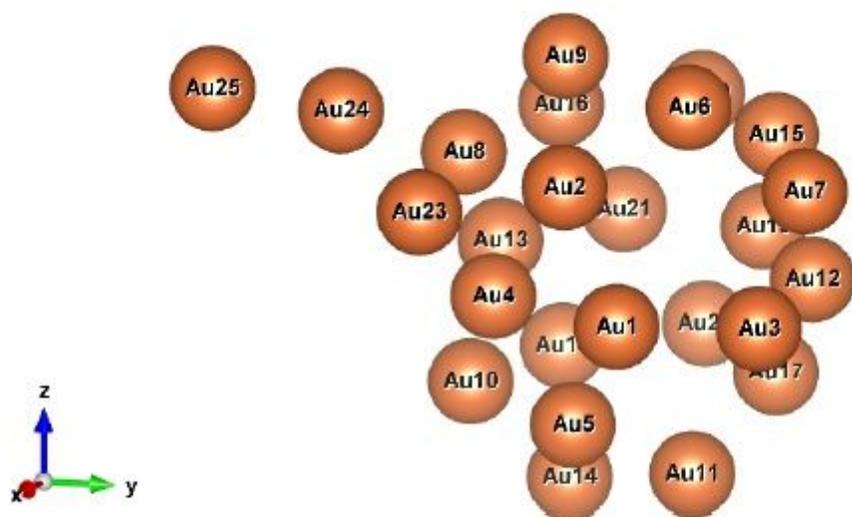
Figure 5

Au25 (C1); Style (Space-lling [above], Polyhedral [below]): The lowest energy geometrical structures of the Au25 cluster. Standard orientation of crystal shape at $\Delta E = 0$.

Supplementary Files

This is a list of supplementary files associated with this preprint. Click to download.

- Au21Au.txt
- Au22Au.txt

- Au23Au.txt
- Au24Au.txt
- Au25Au.txt